



Effective activation energy and phase diagram in the Er-doping MTG-YBa₂Cu₃O_{7-δ} crystal

T. Yang^a, Z.H. Wang^{a,*}, H. Zhang^b, J. Fang^c, Y. Nie^a, L. Qiu^a, S.Y. Ding^a

^a Department of Physics, National Laboratory of Solid State Microstructures, Nanjing University, Nanjing 210093, PR China

^b Shanghai Institute of Metallurgy, Chinese Academy of Sciences, Shanghai 200050, PR China

^c Institute of Plasma Physics, Chinese Academy of Sciences, Hefei 230031, PR China

Received 21 February 2002; received in revised form 2 May 2002; accepted 9 May 2002

Abstract

The resistivity of melted textured growth (MTG) Y_{0.8}Er_{0.2}Ba₂Cu₃O_{7-δ} (YErBCO) crystal has been measured as a function of temperature T , applied magnetic field H and the angle θ between the applied magnetic field and ab -plane. Based on the Yeshurun–Malozemoff model [Phys. Rev. Lett. 60 (1988) 2202], we investigated the vortex dynamic behavior from the Arrhenius form $\rho(T, H) = \rho_0 \exp(-U_0/T)$ and found that the model can explain the dissipation in the vortex liquid state for the Er-doped YBa₂Cu₃O_{7-δ} (YBCO) crystal. The effective activation energies for $H\parallel c$ in the Er-doped MTG-YBCO are about 2.7×10^3 K (7.5 T) and 5.6×10^4 K (0.5 T) less than that for $H\parallel c$ in pure YBCO. The anisotropy factor $\gamma = 10$ obtained from the angular dependencies of effective activation energy $U(\theta)$ and the zero resistance temperature $T_{c0}(\theta)$ for Er-doped YBCO crystal are larger those that for YBCO crystal. The field dependence of the effective activation energy U_e follows a power law, $U_e \propto H^{-\alpha}$, with $\alpha = 1.0$ for $H\parallel c$ and for various angles θ at a fixed magnetic field of 4 T. The phase diagram of the Er-doped YBCO crystal is presented and discussed.

© 2002 Elsevier Science B.V. All rights reserved.

PACS: 74.72.Bk; 74.62.Bh; 74.60.Ge; 74.25.Dw

Keywords: MTG-YErBCO; The effective activation energy; Thermally activated flux creep

1. Introduction

The mixed-state flux dynamics in high- T_c superconductors (HTSCs) is an attractive and complex subject. Much attention has been paid to the relationship between the dissipative flux motion and the flux pinning mechanism, but still many issues are to be resolved [1]. Since there exists

much shorter coherence length ξ and much higher thermal energy $k_B T$ near the superconducting transition in the HTSCs than that in the conventional superconductors, the thermally activated flux motion plays an important role during the onset of the finite resistance. The lower order-of-magnitude U_0 , coupled with the higher T_c s lead to the observed “giant flux creep” [2]. For example, the typical value of $k_B T_c/U_0$ is of order 10^{-3} in conventional low-temperature superconductors, while of order 0.05 in YBa₂Cu₃O_{7-δ} (YBCO) [2]. So the effective activation energy U_e , which measures the depth of the activation energy well, is an

* Corresponding author. Tel.: +86-25-359-3661; fax: +86-25-359-5535.

E-mail address: zhwang@netra.nju.edu.cn (Z.H. Wang).

indispensable parameter for interpretation of the thermally activated motion behaviors in the mixed state.

The doped samples of rare earth elements (Nd, Sm, Eu, Gd, etc.) [3–5] have been intensively studied due to their greater radius of the atoms than Y, which bring about the stronger pinning strength. While Er-doping polycrystalline samples have been studied from the ESR and SLR techniques [6–8], and it is found that there exist the peculiarities of magnetic interactions between Er³⁺-ions and Cu²⁺-spin system on copper-oxide plane [8]. However, the transport property of the textured Er-doped YBCO crystal has rarely performed, so it should be considered for further research. And it is well known that the Yeshurun–Malozemoff model [2] is proved to be suited for the thermally activated flux creep behaviors in typical 2D Bi-2212 [9] and transitional Hg-1223 [10]; while in the case of YBCO [10] with a lower anisotropy ratio, it's found that Tinkham's form [11] was valid. In this paper, we measured the resistivity of melted textured growth (MTG)-Y_{0.8}Er_{0.2}Ba₂Cu₃O_{7- δ} (YErBCO) crystal as a function of temperature, magnetic field and the angle θ between the applied magnetic field and *ab*-plane and analysis the effective activation energy by Y–M model. The result shows that there is a larger TAFF region in the sample. The effect of Er-doping on the flux pinning is discussed in the text.

2. Sample and experimental

The Er-doped YBCO (YErBCO + 40 mol% Y₂BaCuO(211)) crystal used in this study was prepared by the MTG method. The premeditated powders were ground sufficiently to ensure the uniformity of composition, and then calcined at 900 °C for 24 h. The sintered powder was ground again, then pressed into pellets and sintered at 920 °C for 24 h. The same process like the second times has been done for the third times. The pellets were heated to 1050 °C from room temperature at the rate of 200 °C/h and kept for 1 h, then quickly cooled to 1010 °C, followed by a slow cooling to 950 °C at the rate 2 °C/h and later a quick cooling to 600 °C at 50 °C/h, then a furnace-cooling to

room temperature. The samples cleaved from the MTG-YErBCO bulk with a single domain were oxygenated at 400 °C in flowing oxygen gas at 1 atm for more than 50 h for the uniformity of oxygen. A platelet with the size of 8.7 × 4.7 × 0.5 mm³ cut from a larger crystal was held on a rotatable sample holder, where the angle between the applied magnetic field *H* and the surface of the film could be adjusted conveniently and the resolution of the angle was 0.1°. The resistance was performed by standard four-probe technique using the method of plus and minus current. A programmable Keithley 220 current supplier was used as the current source. A Keithley 182 nanovoltmeter was used to detect the voltage signal with a resolution of 2 nV. The magnetic field up to 8 T was supplied by superconducting solenoid magnet system. The temperature was measured by a calibrated Rh–Fe resistance thermometer and corrected for the effect of magnetic field. The zero resistance temperature of the sample is 87.7 K, and the magnetic critical current density *J_c* is 2.4 × 10⁴ A/cm² at 77.3 K in zero magnetic field. The X-ray data, microstructure and magnetization of the sample have been reported elsewhere [12].

3. Results and discussion

3.1. Effective activation energy *U_{eff}* in TAFF region

Fig. 1 shows the temperature dependence of the resistivity at the magnetic field parallel to the *c*-axis up to 7.5 T. The broadening of the resistive transition with the increasing of applied magnetic field is observed obviously. The Arrhenius plots of $\rho(T, H)$ for external magnetic fields from 0.5 to 7.5 T as a function of inversed temperature $1/T$ is shown in the inset of Fig. 1. From the inset of Fig. 1, we can clearly see that the slope $d(\ln \rho)/d(1/T)$ of the Arrhenius plot strongly depends on the temperature. Fig. 2 shows the slope $-d(\ln \rho)/d(1/T)$ versus the temperature at various magnetic fields for $H \parallel c$. We can find that at a fixed field the absolute of slope decreases with the increasing of temperature, showing a linear behavior, below a certain temperature T^* , as indicated by a straight solid line; above the temperature T^* , the slope

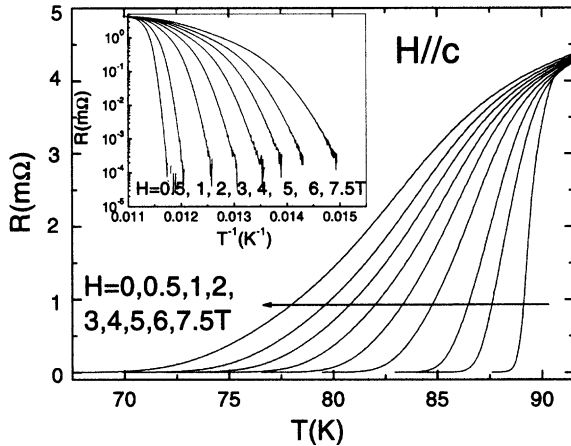


Fig. 1. Resistive transition curves of MTG-YErBCO crystal at magnetic fields up to 7.5 T for $H||c$ with $H \perp J$. Inset displays the inversed temperature dependence of resistance in semi-logarithmic plot.

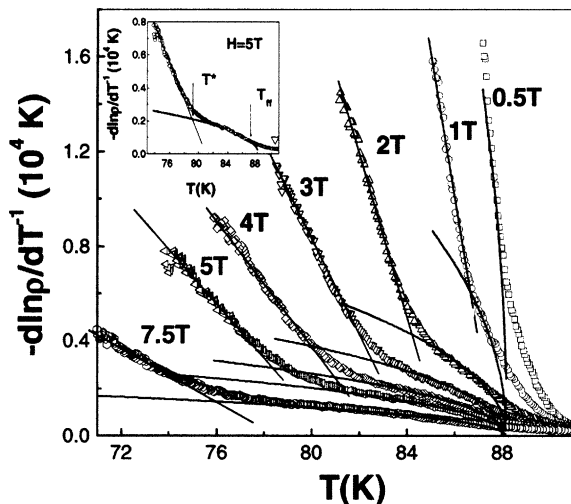


Fig. 2. Temperature dependence of the slope $-d(\ln \rho)/d(1/T)$ of the Arrhenius curve at various magnetic field for $H||c$. The scatter symbols are the experimental data for the various magnetic field. The solid curves are calculated by the equation, $U_c(T, H) = U(H)(1 - T/T_c)^{3/2}[1 + 1.5T/(T_c - T)]$ for the various magnetic field. The straight solid lines are guides for the eyes. Inset shows the definition of T^* and T_{fr} .

increases with the decreasing of temperature, following the Yeshurun–Malozemoff model, as indicated by a solid curve. We defined the crossover from the Y–M model to the straight line as the

characteristic temperature T^* . To keep the picture clear to see, we only mark the position of the temperature at 5 T, indicated by the arrow, in the inset of Fig. 2. The physical meaning of the characteristic temperature T^* will be explained in the following.

It is well known that the thermally activated flux creep can produce dissipation suggested by Palstra et al. [9] as follows:

$$\rho(T, H) = \rho_0 \exp(-U_0/kT) \quad (1)$$

where ρ_0 is the pre-exponential factor independent of field and orientation, k is the Boltzman constant and U_0 is the actual activation energy that generally depends on the temperature T , the current density J and the applied magnetic field H . Generally, the current density dependence of activation energy is a constant when the measuring current density is lower than 10^3 A/cm² [13,14]. From Eq. (1), we can understand that the slope $-d(\ln \rho)/d(1/T)$ of $\ln \rho \sim 1/T$ plot is the effective energy U_{eff} , $U_{eff} = -d(\ln \rho)/d(1/T)$. Therefore, Fig. 2 gives us an information of the activation energy that the value of U_{eff} is slowly increasing with the decreasing of temperature above a certain temperature T^* ; below the temperature T^* , the effective activation energy increases rapidly with the decreasing of temperature, indicating that the flux lines are *softened*. The similar behavior of the activation energy is also reported in HgBCCO samples [10] and BSCCO single crystal [15]. Safar et al. [15] and Carruzzo and Yu [16] claimed that the rapid increasing of effective energy with the decreasing temperature shows the vortex lines into a vortex-glass state. However, the vortex-glass line in the YBCO thin films showed that it is lower than the irreversibility line determined by the criteria of $R/R_n = 0.05\%$ [17]. The characteristic temperature T^* is not consistent with the vortex-glass transition temperature. In addition, we will find that the temperature dependence of pinning energy follows the thermally activated flux creep behavior above the temperature T^* , as shown in Fig. 2. Therefore, we contest that the vortices are softened below the characteristic temperature T^* . The characteristic temperature T^* might be a crossover from the vortex softened state to the thermally activated flux creep state.

In fact, considering the field and temperature dependencies of activation energy U_0 in Eq. (1) at a constant measuring current density, we can write the activation energy as $U_0(H, T) = U(H)U(T) = U(H)(1 - T/T_c)^\beta$. Therefore, we can obtain the effective activation energy,

$$U_{\text{eff}} = -\frac{d \ln \rho}{d(1/T)} = U_0(H, T) - T \frac{dU_0(H, T)}{dT} \\ = U(H) \left(1 - \frac{T}{T_c}\right)^\beta \left[1 + \beta \frac{T/T_c}{1 - T/T_c}\right]. \quad (2)$$

If we accept the temperature dependence of activation energy, $U(T) = (1 - T/T_c)^\beta$ with $\beta = 3/2$, suggested by Yeshurun and Malozemoff in the thermally activated flux flow region, the effective activation energy should be followed in the form,

$$U_{\text{eff}} = U(H) \left(1 - \frac{T}{T_c}\right)^{3/2} \left[1 + \frac{3}{2} \frac{T}{(T_c - T)}\right] \quad (3)$$

where T_c is determined the temperature where the reduced resistance $R/R_n = 0.01$ at zero magnetic field and $U(H)$ is a fitting parameter dependent on the applied magnetic field H . The solid curves presented in Fig. 2 are the temperature dependence of the effective activation energy U_{eff} calculated by Eq. (3) for various magnetic fields. From Fig. 2, we can see that, besides below T^* , there is another deviation of the experimental data from the theoretical curve at a constant magnetic field near the critical temperature. In general, the deviation is considered as the boundary between the thermally activated flux flow and the flux flow region where the temperature was symbolized as T_{ff} in Fig. 2. At the temperature T_{ff} the activation energy starts to become comparable to the thermal T . The boundary has been discussed in YBCO thin films using the transport measurement by Cao et al. [18]. Therefore, we consider the flux lines are in the free flow region above the temperature T_{ff} . Fig. 2 shows that the calculated results fit well with the part of $U_{\text{eff}} \sim T$ curves obtained from the experiment results, indicating that the value of U_c in the limited temperature region $T^* < T < T_{\text{ff}}$ are well described by the theoretical calculation suggested by Yeshurun and Malozemoff [2].

3.2. Anisotropy factor γ

It is also well known that the HTSCs are higher anisotropy. The anisotropy factor is usually defined as $\gamma = (m_c/m_{ab})^{1/2} = \lambda_c/\lambda_{ab} = \xi_{ab}/\xi_c = H_{c2}^{ab}/H_{c2}^c > 1$ [19]. Generally, the anisotropy factor can be determined by the angular dependence of resistive transition curves at a constant magnetic field. According to GL theory, the resistive broadening in the external magnetic field H is equal to that in the effective magnetic field H_e along the c -axis when H tilted away from the ab -plane. The effective magnetic field H_e follows the formula,

$$H_e(\theta) = H(\sin^2 \theta + \cos^2 \theta/\gamma^2)^{1/2} \quad (4)$$

where θ is the angle between the applied magnetic field and the ab -plane.

Combining Eq. (4) with the field dependence of irreversibility temperature T_{irr} , $H = H_0(1 - t)^n$ for $H \parallel c$, we can obtain the angular dependence of the irreversibility temperature $T_{\text{irr}}(\theta)$ at a fixed magnetic field H , expressed by the following form [20,21]:

$$T_{\text{irr}}(H, 0^\circ) - T_{\text{irr}}(H, \theta) \propto H^{1/n} (\sin^2 \theta + \cos^2 \theta/\gamma^2)^{1/2n} \quad (5)$$

Meanwhile, the angular dependence of activation energy U at a fixed magnetic field H can be given in the form

$$U_0(H, \theta) = U(H_e). \quad (6)$$

Fig. 3 shows the temperature dependence of resistance for various angles from -6° to 90° at a constant magnetic field 4 T. The resistive transition becomes broader as the angle increases from 0° to 90° . The inset of Fig. 3 can help us to see clearly the smaller part of resistance values. From Fig. 1, we can also extract the field dependence of the irreversibility temperature T_{irr} , which is defined by the criteria $R/R_n = 0.01\%$, where R_n is the normal state resistance. Fig. 4 displays the information about the relations of T_{irr} and θ . From Fig. 4, we can see that T_{irr} changes monotonously with the increasing of angle θ from 0° to 90° . The cusp happens at 0° .

As shown in Fig. 4, the irreversibility temperature decreases with the increasing of the applied magnetic field H and shows a good power law

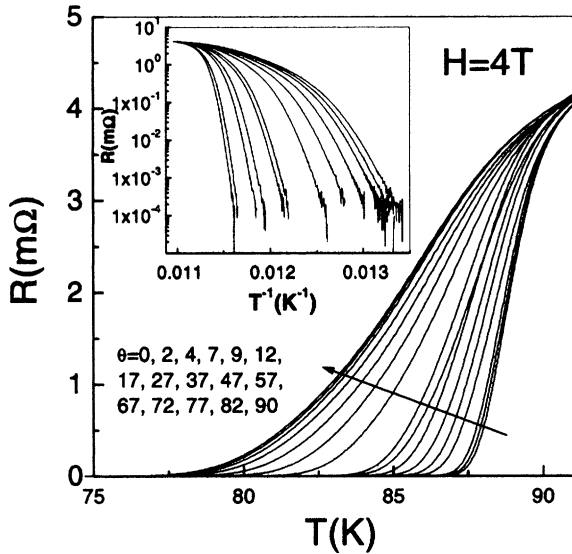


Fig. 3. Angular dependence of the resistive transition curve for various angles θ at a constant magnetic field of 4 T. Inset shows the angular dependence of the resistive transition curve in semi-logarithmic plot.

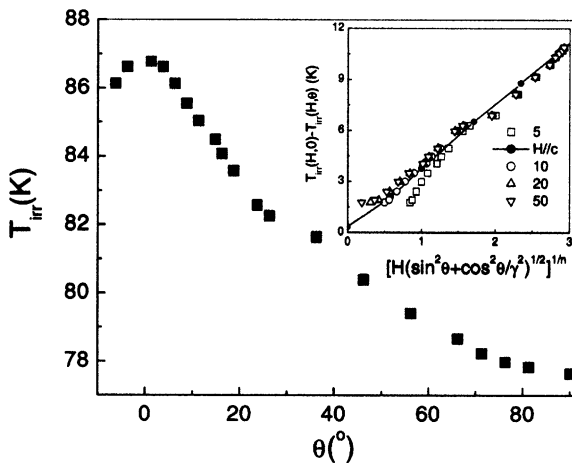


Fig. 4. Angular dependence of irreversibility temperature T_{irr} at a fixed field of 4 T. Inset displays the relationship of $T_{irr}(0) - T_{irr}(H)$ vs $H^{1/n}(\sin^2 \theta + \cos^2 \theta / \gamma^2)^{1/2n}$ with different anisotropy factor γ at 4 T and the field dependence of $T_{irr}(0) - T_{irr}(H)$ for $H \parallel c$.

behavior, $H \propto (T_{irr}(0) - T_{irr}(H))^n$ with $n = 1.29$ for $H \parallel c$, in agreement with the “irreversibility line”, namely, $H \propto (T_c - T_{c0})^{3/2}$.

According to Eq. (5), we can scale the angular dependence of irreversibility temperature at a constant magnetic field with different anisotropy value of $\gamma = 5, 10, 20, 50$, respectively. The scaling of $T_{irr}(H, 0^\circ) - T_{irr}(H, \theta)$ vs $H^{1/n}(\sin^2 \theta + \cos^2 \theta / \gamma^2)^{1/2n}$ displays a good linear behavior only when γ has a value of about 10. It is also consistent with the field dependence of irreversibility temperature for $H \parallel c$. The scaling behavior shows that the anisotropy in the Er-doped YBCO crystal is larger than that in pure YBCO. This result gives us an information that the Er substitution can induce a larger anisotropy.

3.3. Field and angular dependencies of the activation energy $U(H)$

From Fig. 5, we can obtain the temperature dependence of the slope $-(d \ln \rho) / d(1/T)$ of Arrhenius plot for various angles θ at a fixed magnetic field 4 T. The slope behavior of Arrhenius plot for various angles θ is similar to that for $H \parallel c$, as observed in Fig. 2. Therefore, the calculation of effective energy U_e by the Yeshurun–Malozemoff model in the TAFF region is presented for different angle θ , as seen the solid curves of Fig. 5.

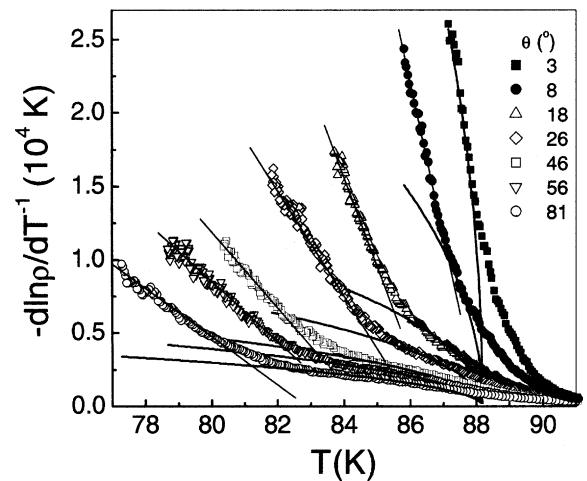


Fig. 5. Temperature dependence of the slope of the Arrhenius curve $U_e = -d(\ln \rho) / d(1/T)$ for various angles θ at a constant magnetic field of 4 T. The scatter symbols are the experimental data for the various angles. The solid curves are calculated by the equation, $U_e(T, H) = U(H)(1 - T/T_c)^{3/2}[1 + 1.5T/(T_c - T)]$. The straight solid lines are guides for the eyes.

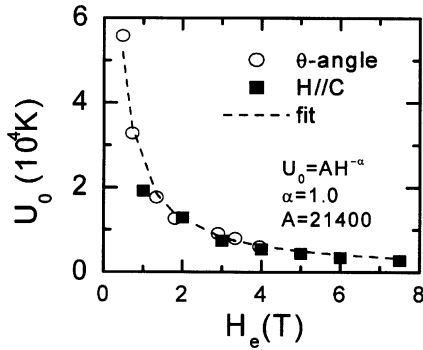


Fig. 6. Field dependence of the fitting parameter $U(H)$ for $H\parallel c$ (solid symbols) and for different angle θ at a fixed field of 4 T. The solid line is the fitting curve, $U = 2.14 \times 10^4 H^{-1}$.

Meanwhile, the value of $U_0(H, \theta)$ from the fitting process was obtained for various angles θ .

Fig. 6 shows the field dependence of the fitting parameter $U(H)$ for $H\parallel c$ and/or for H_e at a fixed field of 4 T. From Fig. 6, the magnitude of the effective energy U for the YErBaCuO crystal is around from 2.7×10^3 K at 7.5 T to 5.6×10^4 K at 0.5 T for $H\parallel c$, a little less than that for YBCO [9]. In order to compare the consistence of field dependence of activation energy for $H\parallel c$ with that for various angles θ , we plot the effective magnetic field of activation energy with different anisotropic factor γ . The angular dependence of activation energy with $\gamma \approx 10$ is quantitatively consistent with the field dependence of that for $H\parallel c$. The value of $U(H)$ decreases with the increasing of applied magnetic field and follows a power law behavior, $U = AH^{-\alpha}$ with $A = 2.14 \times 10^4$ K and $\alpha \approx 1.0$. The dash line in Fig. 6 is the fitting line. From this figure the results in the effective magnetic field H_e when H tilted away from the CuO_2 plane, are consistent with those when $H\parallel c$. As reported by Yeshurun and Malozemoff [2], we can get the intrinsic planar pinning and extrinsic point pinning from the magnetic field behavior of activation energy, $U \propto H^{-\alpha}$. $\alpha = 0.5$ and 1 are responsible for the intrinsic planar pinning and extrinsic point pinning, respectively. For our sample, $\alpha \approx 1.0$ indicates that the extrinsic point pinning is main flux pinning. The extrinsic point pinning might be resulted from the Er addition. The Er^{3+} substitution for Y^{3+} possibly destroyed the strength of coupling

between the CuO_2 because of the highly anisotropic g value in Er^{3+} ions [8] and changed the anisotropy of the sample.

3.4. Phase diagram in Er-doped MTG-YBCO crystal

According to above discussions, the field dependence of the characteristic temperature T^* , T_{ff} and the irreversibility temperature T_{irr} can be drawn in a picture, as shown by the solid symbols in Fig. 7. The field dependence of T_{ff} , T^* and T_{irr} follows the same behavior $H \propto (1 - t)^n$ with $n = 1.29$. The angular dependence of T_{ff} , T^* and T_{irr} at a fixed magnetic field for different angle θ is also shown by the open symbols in Fig. 7. From Fig. 7, we can see that the phase diagram of Er-doped MTG-YBCO crystal is separated into several regions, namely flux flow, thermally activated flux flow, flux softened and vortex solid regions by three lines of $H-T_{\text{ff}}$, $H-T^*$ and $H-T_{\text{irr}}$. At a fixed magnetic field, when the temperature decreases from above T_c , the vortex lines firstly undergo a transition from flux flow to thermally activated flux creep. In the region, the extrinsic point defects might be main flux pinning centers. As the temperature decreases further, the flux lines go through a transition from thermally activated flux creep to the softened vortices. When the vortices are softened, the pinning energy increases rapidly with the decreasing

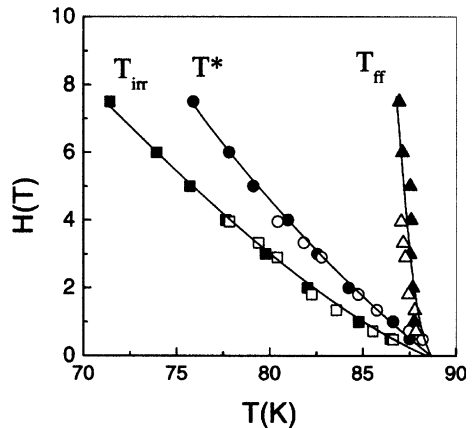


Fig. 7. Vortex phase diagram for MTG-YErBCO crystal. The solid symbols are for $H\parallel c$ and the open symbols are at a fixed field of 4 T for different angle θ .

temperature. In the region, the co-action of point defects and planar defects is responsible for the flux pinning [12]. In final, the vortex lines go into solid below the irreversibility temperature, T_{irr} . The existence of flux softened region might indicate that the melting transition of flux lines is a second order phase transition [22,23] in our sample with correlated disordered defects. Compared with the typical 2D BSCCO T^* ($\approx 0.45T_c$) [15] and the transitional Hg-1223 T^* ($\approx 0.65T_c$) [10] in 5 T, the T^* value of YErBCO is about $0.92T_c$. The width ΔT of the TAFF region at 5 T is about 18 K in Hg-1223 [10] and 8.4 K in YErBCO crystal, respectively. These comparisons show the much narrower TAFF region in YErBCO crystal.

4. Conclusions

We have measured the resistance property of Er-doped MTG-YBCO crystals as a function of temperature and magnetic field H up to 7.5 T. The field dependence of effective activation energy for $H\parallel c$ is consistent with the effective magnetic field dependence of effective activation energy at a fixed field of 4 T for different angle θ . Er³⁺ substitution for Y³⁺ increases the anisotropy of the MTG-YBCO sample possibly because of the highly anisotropic g -value of Er. The effective activation energy is discussed by the Yeshurun–Malozemoff model. The results indicate that the phase diagram of Er-doped MTG-YBCO crystal can be separated into four regions, namely flux flow, thermally activated creep, soft vortex liquid and vortex solid regions by three lines of $H-T_{\text{ff}}$, $H-T^*$ and $H-T_{\text{irr}}$. In the thermally activated creep region, the extrinsic point defects might be main flux pinning centers. In the soft vortex liquid region, the co-action of point defects and planar defects is responsible for the flux pinning.

Acknowledgements

This work is supported by the National Natural Science Foundation of China (NNSFC-10174033),

the Ministry of Science and Technology of China (NKBRF-G1999064602) and Nanjing University Talent Development Foundation.

References

- [1] L.F. Cohen, H.J. Jensen, Rep. Prog. Phys. 60 (1997) 1581.
- [2] Y. Yeshurun, A.P. Malozemoff, Phys. Rev. Lett. 60 (1988) 2202.
- [3] S.I. Yoo, N. Sakai, I.L. Takaichi, M. Murakami, Appl. Phys. Lett. 65 (1994) 633.
- [4] M. Muralidhar, H.S. Chauhan, T. Saitoh, K. Segawa, K. Kamada, M. Murakami, Supercond. Sci. Technol. 10 (1997) 663.
- [5] M. Muralidhar, M.R. Koblishka, T. Saitoh, M. Murakami, Supercond. Sci. Technol. 11 (1998) 1349.
- [6] H. Shimizu, K. Fujiwara, K. Hatada, Physica C 282–287 (1997) 1349.
- [7] M.X. Huang, J. Barak, S.M. Bhagat, L.C. Gupta, A.K. Rajarajan, R. Vijayaraghavan, J. Appl. Phys. 70 (1991) 5754.
- [8] V.A. Ivanshin, M.R. Gafurov, I.N. Kurkin, S.P. Kurzin, A. Shengelaya, H. Keller, M. Gutmann, Physica C 307 (1998) 61.
- [9] T.T.M. Palstra, B. Batlogg, R.B. van Dover, L.F. Schneemeyer, J.V. Waszczak, Phys. Rev. B 41 (1990) 6621.
- [10] W.-s. Kim, W.N. Kang, M.-S. Kim, S.-I. Lee, Phys. Rev. B 61 (2000) 11317.
- [11] M. Tinkham, Phys. Rev. Lett. 61 (1988) 1658.
- [12] Z.H. Wang, X.W. Zou, J. Fang, T. Yang, Y.L. Tang, Z. Huang, L. Qiu, J.L. Chen, H. Zhang, S.Y. Ding, Supercond. Sci. Technol. 15 (2002) 183.
- [13] Z.H. Wang, K.B. Li, J. Fang, J.L. Chen, X.W. Cao, Z. Phys. B 104 (1997) 445.
- [14] Z.H. Wang, H. Zhang, Physica C 320 (1999) 218.
- [15] H. Safar, P.L. Gammel, D.J. Bishop, D.B. Mitzi, A. Kapitulnik, Phys. Rev. Lett. 68 (1992) 2672.
- [16] H.M. Carruzzo, C.C. Yu, Phil. Mag. B 77 (1998) 1001.
- [17] Z.H. Wang, J. Fang, K.B. Li, Z.Y. Chen, X.W. Cao, Physica C 282–287 (1997) 2131.
- [18] X. Cao, Z. Wang, K. Li, Phys. Rev. B 62 (2000) 12522.
- [19] J.R. Clem, Supercond. Sci. Technol. 11 (1998) 909.
- [20] Z.H. Wang, X.W. Zou, T. Yang, H. Zhang, J. Fang, Z. Huang, L. Qiu, J.L. Chen, S.Y. Ding, Physica C 366 (2002) 195.
- [21] Z.H. Wang, S.A. Aruna, S.Y. Ding, X.W. Cao, Supercond. Sci. Technol. 13 (2000) 1509.
- [22] D.S. Fisher, M.P.A. Fisher, D.A. Huse, Phys. Rev. B 43 (1991) 130.
- [23] C.P. Bean, Phys. Rev. Lett. 8 (1962) 250.